JVR
Journal of
Vascular Research

Research Article

J Vasc Res
DOI: 10.1159/000531584

Received: December 2, 2022
Accepted: March 14, 2023
Published online: June ■■■, 2023

Tortuosity and Proximal-Specific Hemodynamics Associated with Plaque Location in the Carotid Bulb Stenosis

Lei Ren[a, b, c] Rongjie Xu[d] Chenxi Zhao[a] Wenfei Li[a, e] Shu Wang[f, g, h, i] Chen Cao[j] Yan Gong[k] Jinxia Zhu[l] Xuequan Feng[m] Bo Ren[d] Shuang Xia[n]

[a]Department of Radiology, First Central Clinical School, Tianjin Medical University, Tianjin, China; [b]Department of Radiology, First Teaching Hospital of Tianjin University of Traditional Chinese Medicine, Tianjin, China; [c]National Clinical Research Center for Chinese Medicine Acupuncture and Moxibustion, Tianjin, China; [d]College of Computer Science, Nankai University, Tianjin, China; [e]Department of Radiology, First Hospital of Qinhuangdao, Qinhuangdao, China; [f]Department of Breast Oncoplastic Surgery, Tianjin Medical University Cancer Institute and Hospital, Tianjin, China; [g]National Clinical Research Center for Cancer, Tianjin, China; [h]Key Laboratory of Breast Cancer Prevention and Therapy, Tianjin Medical University, Ministry of Education, Tianjin, China; [i]Key Laboratory of Cancer Prevention and Therapy, Tianjin's Clinical Research Center for Cancer, Tianjin, China; [j]Department of Radiology, Tianjin University Huanhu Hospital, Tianjin, China; [k]Department of Radiology, Tianjin Nankai Hospital, Tianjin, China; [l]MR Collaboration, Siemens Healthineers Ltd., Beijing, China; [m]Department of Neurosurgery, Tianjin First Central Hospital, School of Medicine, Nankai University, Tianjin, China; [n]Department of Radiology, Medical Imaging Institute of Tianjin, Tianjin First Central Hospital, School of Medicine, Nankai University, Tianjin, China

Keywords
Atherosclerosis · Computational fluid dynamics · Carotid bulb · Plaque location · Wall shear stress

Abstract
Background: Atherosclerotic plaque locations in the carotid bulb increasingly have been found to be associated with patterns of ischemic lesions and plaque progression. However, the occurrence of carotid bulb plaque is a complex process. We aimed to investigate plaque characteristics and geometric and hemodynamic parameters among patients with body and apical plaques of the carotid bulb and to identify the mechanism of bulb plaque formation and location. ***Methods:*** Consecutive patients with single carotid bulb stenosis (50–99%) were enrolled retrospectively. Patients were divided into body and apical plaque groups based on plaque location. Plaque location and characteristics were identified and measured on high-resolution vessel wall magnetic resonance imaging. Geometric parameters were derived from time-of-flight magnetic resonance imaging. Computational fluid dynamics simulations were performed to quantify wall shear stress (WSS) and four associated WSS-based metrics on the plaque side, on the non-plaque side, and in different parts of the lesion. Plaque characteristics and geometric and hemodynamic parameters were compared, and their associations with the plaque location were determined. ***Results:*** Seventy patients were recruited (41 body plaques and 29 apical plaques). WSS_{plaque} values were lower than $WSS_{non\text{-}plaque}$ values for all plaques (median [interquartile range], 12.59 [9.83–22.14] vs. 17.27

Lei Ren, Rongjie Xu, and Chenxi Zhao contributed equally and share first authorship.

Correspondence to:
Shuang Xia, xiashuang77@163.com

[11.63–27.63] Pa, $p = 0.001$). In a multivariate binary logistic regression, the tortuosity of the stenosed region, the magnitudes of the mean relative residence time, and the minimum transverse WSS in the proximal part of the lesion were the key factors independently associated with plaque location ($p = 0.022$, 0.013, and 0.012, respectively). ***Conclusions:*** Plaque formation was associated with the local flow pattern, and the tortuosity and proximal-specific hemodynamics were significantly associated with plaque location in the carotid bulb.

Introduction

Carotid artery atherosclerotic stenosis occurs when a plaque narrows the vessel lumen, an event that is prevalent in the carotid bulb and is increasingly considered the leading cause of ischemic stroke [1, 2]. Plaque locations in the stenotic carotid bulb can be divided into body plaque and apical plaque according to anatomical features [3]. Previous studies have demonstrated that bulb plaque location is associated with the progression of plaque formation [4]. Hyperlipidemia and a lesion pattern of small, scattered ischemic lesions occur more frequently in patients with body plaques [3, 5]. Consequently, plaque location has drawn increasing clinical attention as an important indicator and mechanism of ischemic stroke.

High-resolution vessel wall imaging (HR-VWI) has been shown to be of use in evaluating the location and characteristics of carotid plaques [6, 7]. The combination of patient-specific geometric models extracted from medical imaging modalities and finite element-based computational fluid dynamics (CFD) has emerged as an important tool for the estimation of hemodynamics [8]. The geometric properties of the carotid artery have been reported to be associated with plaque occurrence [9–11]. For example, potentially atherogenic flow conditions occur predominantly at the proximal internal carotid artery (ICA) [12], and carotid atherosclerotic plaques tend to occur near arterial bifurcations or bends.

Low and oscillatory wall shear stresses (WSS) have long been considered risk factors for atherosclerosis [13]. Previous histopathological studies have shown significant differences in plaque surface conditions between the upstream and downstream of the stenosis [14]; it can be deduced that the flow status near the plaques is different among the proximal part, the distal part, and the most severely narrowed level (NL). Nevertheless, some controversy persists. Some studies found that the high WSS appeared on the plaque shoulders, whereas others found the maximum values appeared at the top of plaque hills, as well as the thrombus region and the thickest region of plaque [15]. Few studies of this field have assessed plaque characteristics via HR-VWI. Moreover, descriptors of the complex multidirectional nature of WSS have been proposed, i.e., transverse WSS (transWSS, calculated as the time average of wall shear stress components perpendicular to the mean flow direction), a new multidirectional WSS metric, may be important in atherosclerosis development [16]. However, few studies of this field have assessed transWSS and other multidirectional WSS metrics on different parts of the carotid bulb atherosclerotic lesion.

The present study sought to test the hypothesis that differences in the local flow pattern are an important mechanism for plaque formation in carotid bulb stenosis. Besides hemodynamics, geometry and plaque characteristics may be associated with plaque location. Our goals included the following: (1) to visually and quantitatively evaluate the specific local flow pattern around plaque in carotid bulb stenosis; (2) to further demonstrate the relationships between hemodynamics, geometry, plaque characteristics, and plaque location; (3) to investigate whether hemodynamics and geometry can provide an incremental contribution to different plaque locations.

Materials and Methods

Study Participants

This was a retrospective cross-sectional study, from September 2016 to March 2021, and 346 patients with carotid bulb stenosis were analyzed in a HR-VWI and magnetic resonance angiography (MRA) database in Tianjin First Central Hospital. Patients with single atherosclerotic plaque in carotid bulb stenosis (50–99%) were included. The degree of stenosis was defined as 50–99% as detected by MRA, according to the guidelines of the North American Symptomatic Carotid Endarterectomy Trial (NASCET). The detailed inclusion and exclusion criteria are presented in Figure 1. Patient demographics and vascular risk factors were collected during patient hospitalization.

Imaging Examination

Patients were scanned with a 3-T magnetic resonance imaging machine (MAGNETOM Prisma; Siemens Healthcare, Erlangen, Germany) with a 64-channel head coil. The protocol for each patient included inversion-recovery-prepared sampling perfection with application-optimized contrast using different flip angle evolutions (IR-SPACE) and time-of-flight MRA. The detailed imaging parameters are provided in the online supplementary material (for all online suppl. material, see https://doi.org/10.1159/000531584).

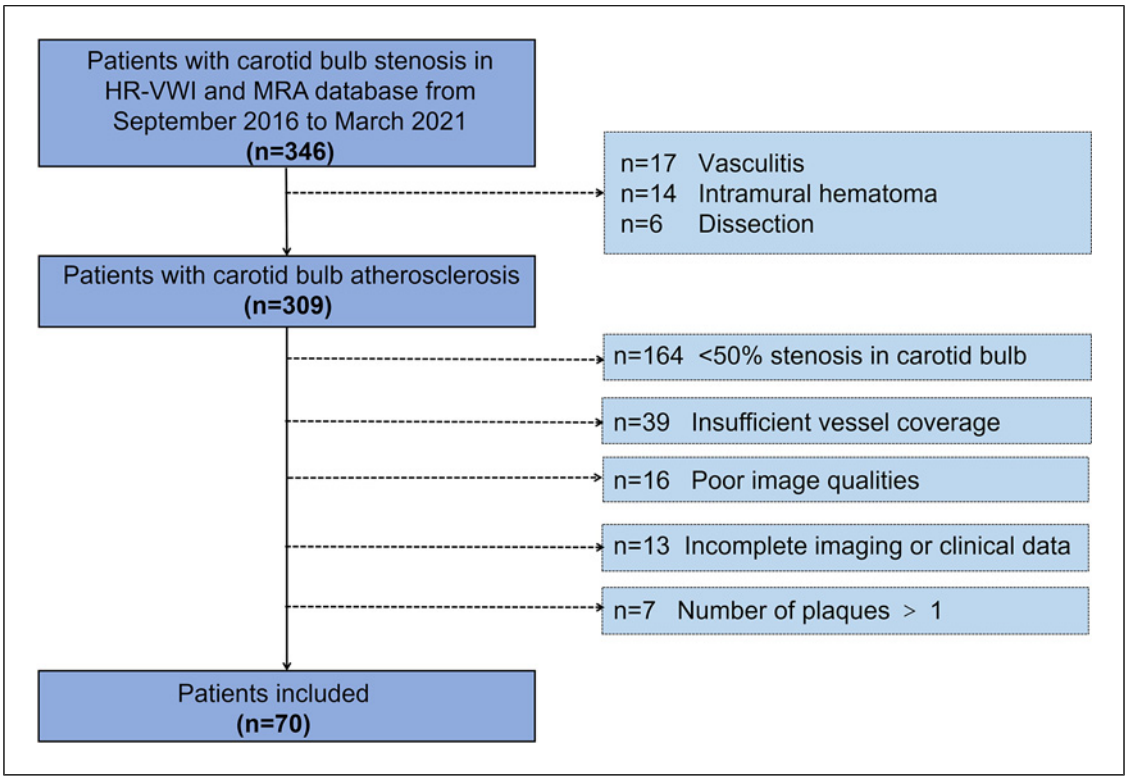

Fig. 1. Flow chart of the study population. HR-VWI, high-resolution vessel wall imaging; MRA, magnetic resonance angiography.

Plaque Characteristic Analysis

Quantitative and qualitative analyses of plaque characteristics and plaque location were performed on IR-SPACE sequences by two independent neuroradiologists with >3 years' experience each. As described in previous studies [17], the degree of stenosis, plaque length, maximum wall thickness (WT), and the percent wall volume (%WV) were determined, and the presence of plaque composition and high-risk plaque were identified [18]. The details of the plaque characteristics are shown in Figure 2a. Based on the involvement of the carotid bulb, body plaques were regarded as plaques in the transitional zone of the bulb and common carotid artery, and apical plaques were regarded as plaques in the transitional zone of the bulb and the proximal cervical ICA segment, respectively. Specially, for differentiation of extended plaques, the location of the main involvement area of the plaque and the level of the most severe stenosis were considered [3, 5]. The anatomic definitions are shown in Figure 2b. Strong interreader reproducibility was obtained for both plaque characteristics and plaque location (intraclass correlation coefficient: 0.86–0.97).

Geometry Reconstruction and Analysis

Geometry reconstruction was derived from the MRA images. A segmentation protocol was established using 3D Slicer (version 4.11; https://www.slicer.org), an open-source software, to identify the boundaries of the arterial lumen and employed to generate a three-dimensional (3D) model from the two-dimensional contours. The reconstructed 3D vessel model was used for both geometry and CFD analysis. Then, using the vascular modeling toolkit extension, similar to prior studies [19, 20], geometric parameters were further calculated. They included (a) bifurcation angle, calculated as the angle between the projections of ICA and external carotid artery vectors onto the bifurcation plane; (b) ICA planarity, calculated as the angle between the out-of-bifurcation plane components of the common carotid artery and ICA vectors; and (c) the tortuosity of the stenosed region, an emerging descriptor of carotid stenosis, calculated using the following formula between the vessel centerline at the proximal and distal ends of the stenosed region: centerline length/Euclidean distance-1. An illustration of all the geometric parameters is provided in online supplementary Figure 1.

Computational Fluid Dynamics and Analysis

The above vascular lumen models were imported into ICEM (ANSYS Inc., Canonsburg, PA, USA) software, and to conduct finite volume analyses, a tetrahedral mesh was used to represent discretization in the physical domain, facilitating the calculation of the numerical solution. Finite-element meshes comprised approximately 560,000 tetrahedral elements on average, with a maximal element size of 0.3 mm, which has previously been shown to be sufficient for resolving wall shear stresses in the carotid bifurcation models [21]. The blood flow simulation was fulfilled by solving the Navier-Stokes and continuity equations in Fluent (ANSYS). Blood flow was assumed to be a laminar, incompressible, and Newtonian fluid, with a density of 1,050 kg/m^3 and a viscosity of 0.0035 Pa*s [22]. To ensure fully developed velocity profiles at the inlet and to

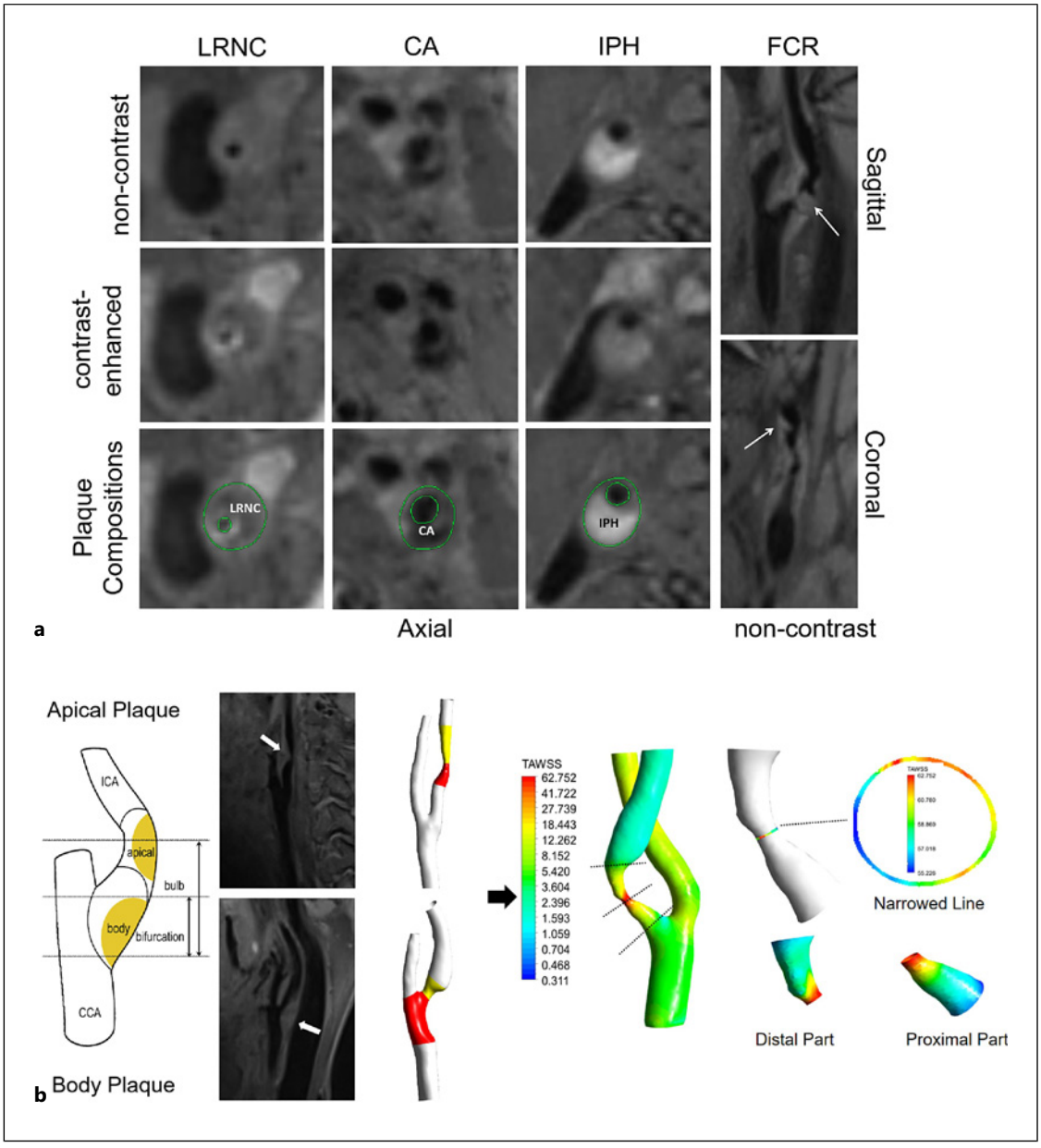

Fig. 2. Evaluation of plaque compositions on HR-VWI and schematic diagram of the study design. **a** From the left to right column are plaques with lipid-rich necrotic core (LRNC), calcification (CA), intraplaque hemorrhage (IPH), and fibrous cap rupture (FCR). **b** Schematic diagram of the study design. Plaque locations are divided into body and apical plaques. Wall shear stress metrics simulated by CFD analysis are measured in three regions: (1) the proximal part of the lesion (between the first normal diameter proximal to the stenosis and the most severely NL); (2) the distal part of the lesion (between the first normal diameter distal to the stenosis and the most severely NL); and (3) the most severely NL. HR-VWI, high-resolution vessel wall imaging; CFD, computational fluid dynamics.

minimize the influence of outlet boundary conditions, flow extensions of the inlet and outlets were set to extend at least five diameters of upstream and downstream of the bifurcation, respectively [13]. The user-defined function of velocity was edited based on the ultrasound centerline velocity measurements made at the common carotid inlets of twenty healthy volunteers. A 3-cycle normalized pulsatile mass flow rate was set at the extended inlet (online suppl. Fig. 2), and zero pressure was set at the extended outlets [23]. No slip and rigid boundary conditions were imposed at the walls. The simulation time step size was set to 0.01 s, running 267 steps (2.67 s, equal to 3 cardiac cycles); the resulting data from the third cardiac cycle were used for post-processing and data

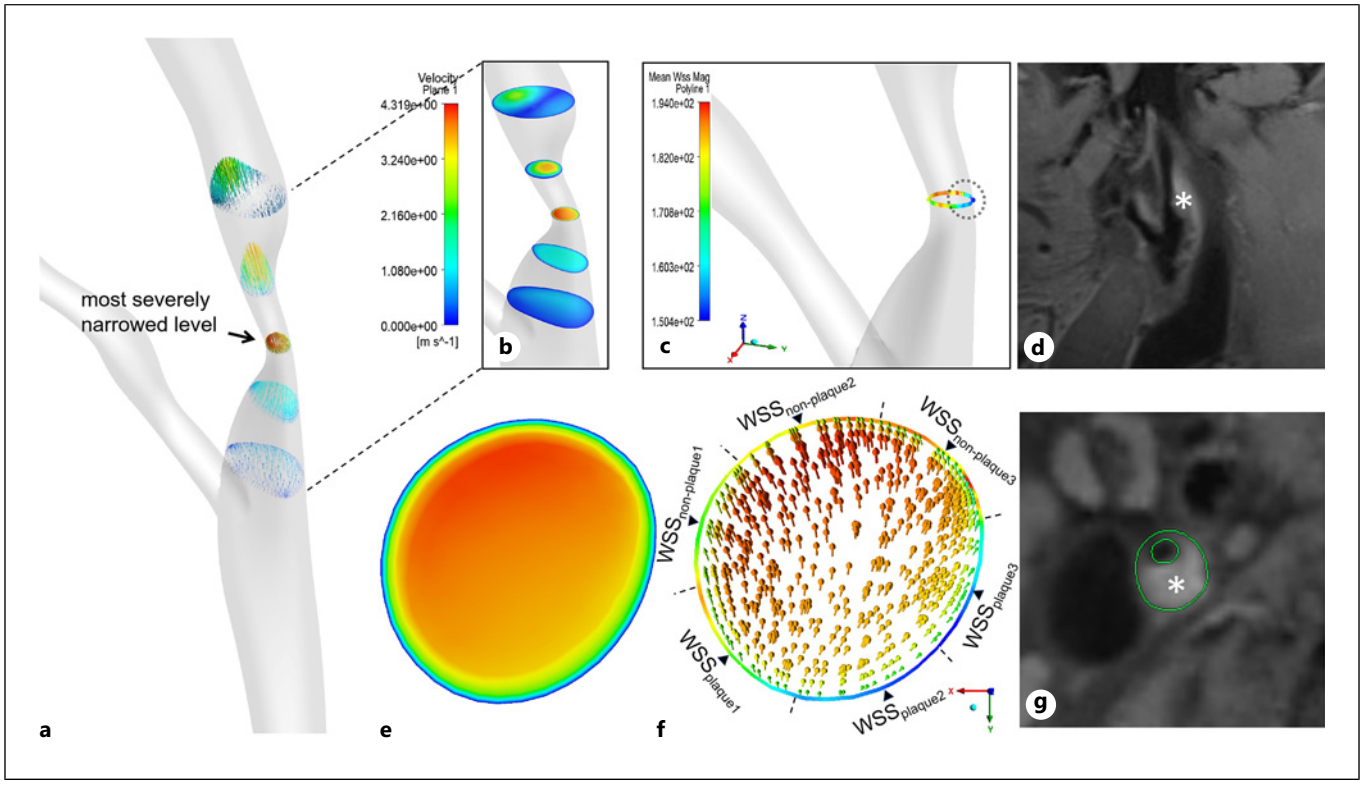

Fig. 3. Distribution of TAWSS magnitude, velocity, and vector direction in the stenosed carotid bulb. TAWSS and velocity are presented as color coded, vector direction is presented as arrows. Contour plots of velocity axial cut planes with in-plane velocity vectors (**a**) and velocity magnitude (**b**) of the stenosed segment. Flow is represented as low velocity (short blue) vectors upstream and downstream of stenosis; flow demonstrates increased velocity at the most severely NL cross-section (**e**). The lumen TAWSS contour at the position of the most severely NL, visualized from different angles (**c**, **f**), corresponding to sagittal (**d**) and axial (**g**) slices (respectively) of HR-VWI. Plaque presents in the area (dotted line) where a decrease in the WSS value is accompanied by low flow velocity (in-plane velocity vectors), rather than around the high WSS zone. TAWSS, time-averaged wall shear stress; HR-VWI, high-resolution vessel wall imaging; WSS, wall shear stress.

analysis. The lumen time-averaged WSS (TAWSS) contour at the position of the most severely NL was divided into plaque side and non-plaque side according to the plaque boundary on HR-VWI. Each side was then equally divided into three regions, and the center point of each region was then measured. WSS_{plaque} and $WSS_{non\text{-}plaque}$ were defined as the mean values of TAWSS at the three center points on the plaque side and non-plaque side, respectively. Following the methods of Gallo et al. [13], maximum, minimum, and mean values of four WSS-based metrics were measured: the TAWSS magnitude, oscillatory shear index (OSI), relative residence time (RRT), and transWSS. We specifically analyzed the hemodynamics in the proximal part, distal part, and the most severely NL of the lesion. Details of the CFD analysis are provided in Figure 2b and online supplementary materials.

Statistical Analysis

Continuous variables were reported as mean ± standard deviation or median with interquartile range (IQR), and categorical variables were reported as proportions. Patient demographics, risk factors, plaque characteristics, and geometric and hemodynamic parameters were compared among patients grouped by plaque location. χ^2 tests were used for categorical variables. Independent-sample *t* test and Mann-Whitney U test were used for continuous variables. Univariate logistic analysis was performed to assess the association between each variable and body plaque. Multivariate binary logistic regression analysis incorporated variables that had $p < 0.05$ in the univariate analysis. The receiver operating characteristic curve was used to evaluate the efficacy of each variable and combination included in the multivariate analysis for the diagnosis of the presence of body plaque. A comparison of the difference in the area under the curve (AUC) between the variables was evaluated using the *Z* test. All statistical analyses were performed using SPSS software (IBM Version 28.0, Chicago). $p < 0.05$ was considered statistically significant.

Results

Patient Demographics

A total of 70 patients with single plaque (mean ± standard deviation age, 66 ± 7 years; 58 men) were included in the final analysis; 41 and 29 patients were

Table 1. Comparison of plaque characteristics and geometric parameters between patients with body and apical plaque in the carotid bulb

Parameters	All n = 70	Body plaque n = 41	Apical plaque n = 29	p value
Mean±SD or n (%)				
Plaque characteristics				
Stenosis, %	64.02±10.20	65.36±10.48	62.13±9.66	0.193
Maximum WT, mm	5.53±1.40	6.05±1.46	4.80±0.92	<0.001*
Plaque length, mm	15.31±5.45	16.64±4.90	13.43±5.71	0.014*
%WV, %	79.68±8.70	79.75±8.50	79.58±9.13	0.943
Presence of calcification	43 (61.43)	28 (68.29)	15 (51.72)	0.161
Presence of LRNC	17 (24.29)	13 (31.70)	4 (13.79)	0.189
Presence of IPH	25 (35.71)	17 (41.46)	8 (27.59)	0.233
Presence of FCR	4 (5.71)	1 (2.44)	3 (10.34)	0.189
Presence of high-risk plaque	41 (58.57)	27 (65.85)	14 (48.28)	0.141
Geometric parameters				
Bifurcation angle, degree	51.76±9.33	51.60±10.36	51.99±7.82	0.863
ICA planarity, degree	14.03±12.94	15.23±14.10	14.03±13.62	0.388
Tortuosity of the stenosed region, %	8.94±6.20	11.07±6.47	5.92±4.34	<0.001*

Maximum WT, maximum wall thick; %WV, percent wall volume; LRNC, lipid-rich necrotic core; IPH, intraplaque hemorrhage; FCR, fibrous cap rupture; ICA, internal carotid artery; SD, standard deviation. *p < 0.05.

classified into groups with body plaque or apical plaque, respectively. We found no evidence of a statistically significant difference between the two groups in terms of sex, age, or carotid stenosis risk factors (including hypertension, diabetes mellitus, coronary artery disease, prior stroke, smoking, and alcohol use) (p > 0.05).

Local Flow Pattern of Plaque Formation

Plaque presented around the area where a decrease in the WSS value was accompanied by low flow velocity. In addition, the flow pattern at the most severely NL was characterized by laminar flow. Each narrowest cross-sectional level of lumen was divided into plaque side and non-plaque side according to the plaque boundary to quantify local WSS. Hence, WSS_{plaque} and $WSS_{non\text{-}plaque}$ values were measured for all 70 plaques. WSS_{plaque} values were lower than $WSS_{non\text{-}plaque}$ values (median [IQR], 12.59 [9.83–22.14] Pa vs. 17.27 [11.63–27.63] Pa; p = 0.001). A representative case is shown in Figure 3.

Plaque Characteristics and Geometric Parameters between Groups with Body and Apical Plaques

Body plaques (compared to apical plaques) had greater maximum values for WT (6.05 ± 1.46 mm vs. 4.80 ± 0.92 mm, respectively; p < 0.001) and plaque length (16.64 ± 4.90 mm vs. 13.43 ± 5.71 mm; p = 0.014). No statistically significant differences were detected for stenosis, %WV, or other plaque characteristics (Table 1). In addition, as listed in Table 1, tortuosity of the body plaques' stenosed region (compared to apical plaques) was greater (11.07 ± 6.47% vs. 5.92 ± 4.34%, respectively; p < 0.001). No statistically significant differences were detected in other geometric parameters.

Hemodynamic Parameters between Groups with Body and Apical Plaques

In general, significant hemodynamic differences between the two groups were found in two WSS-based metrics (RRT and transWSS) of the proximal part and the most severely NL of the lesion. Specifically, the body plaque group (compared to the apical plaque group) exhibited lower values in the proximal part of the lesion for OSI (median [IQR], 0.004 [0.001–0.02] vs. 0.01 [0.001–0.04], respectively; p = 0.022), RRT (median [IQR], 0.13 [0.09–0.21] Pa^{-1} vs. 0.17 [0.09–0.54] Pa^{-1}; p = 0.011), and minimum transWSS (median [IQR], 0.09 [0.05–0.13] Pa vs. 0.15 [0.07–0.22] Pa; p = 0.006). In the most severely NL, the body plaque group (compared to the apical plaque group) had higher maximum OSI (median [IQR], 0.03 [0.01–0.20] vs. 0.001 [0.001–0.006], respectively; p = 0.021) and RRT (median [IQR], 0.05 [0.02–0.12] Pa^{-1} vs. 0.03 [0.02–0.04] Pa^{-1}; p = 0.023). A comparison of the hemodynamic parameters of the two groups is shown in Table 2.

Table 2. Comparison of hemodynamic parameters between patients with body and apical plaque in the carotid bulb

Parameters median [25–75p]	All n = 70	Body plaque n = 41	Apical plaque n = 29	p value
Proximal part of the lesion				
Maximum TAWSS, Pa	82.31 [61.06–136.75]	81.65 [63.98–150.40]	87.72 [58.83–137.30]	0.416
Minimum TAWSS, Pa	0.69 [0.36–1.86]	0.69 [0.37–1.47]	0.90 [0.28–2.28]	0.432
Mean TAWSS, Pa	14.27 [9.40–19.79]	14.20 [9.98–19.78]	14.34 [7.54–21.67]	0.488
Maximum OSI	0.36 [0.22–0.46]	0.39 [0.18–0.44]	0.31 [0.15–0.44]	0.297
Minimum OSI	0.001 [0.0007–0.006]	0.001 [0.0008–0.005]	0.001 [0.0006–0.007]	0.841
Mean OSI	0.007 [0.001–0.02]	0.004 [0.001–0.02]	0.01 [0.001–0.04]	0.022*
Maximum RRT, Pa^{-1}	1.66 [0.60–7.10]	1.73 [0.90–6.91]	1.54 [0.45–13.79]	0.084
Minimum RRT, Pa^{-1}	0.01 [0.007–0.02]	0.01 [0.007–0.02]	0.01 [0.007–0.02]	0.771
Mean RRT, Pa^{-1}	0.14 [0.09–0.26]	0.13 [0.09–0.21]	0.17 [0.09–0.54]	0.011*
Maximum transWSS, Pa	39.63 [29.90–55.05]	40.19 [30.21–67.69]	37.18 [27.16–49.90]	0.214
Minimum transWSS, Pa	0.10 [0.06–0.17]	0.09 [0.05–0.13]	0.15 [0.07–0.22]	0.006*
Mean transWSS, Pa	5.05 [3.28–6.81]	5.19 [3.66–6. 50]	4.80 [2.26–7.30]	0.237
Distal part of the lesion				
Maximum TAWSS, Pa	98.51 [59.38–151.93]	95.29 [55.75–156.90]	108.00 [64.25–140.40]	0.532
Minimum TAWSS, Pa	0.344 [0.16–0.61]	0.33 [0.14–0.53]	0.41 [0.22–0.70]	0.843
Mean TAWSS, Pa	12.16 [6.87–24.18]	9.42 [6.50–18.79]	13.84 [10.75–24.43]	0.763
Maximum OSI	0.40 [0.21–0.43]	0.37 [0.21–0.44]	0.44 [0.24–0.47]	0.266
Minimum OSI	0.008 [0.002–0.01]	0.009 [0.002–0.04]	0.004 [0.001–0.03]	0.648
Mean OSI	0.03 [0.01–0.06]	0.04 [0.01–0.05]	0.03 [0.01–0.04]	0.228
Maximum RRT, Pa^{-1}	9.80 [4.74–24.90]	10.74 [5.07–49.09]	9.06 [3.68–17.17]	0.147
Minimum RRT, Pa^{-1}	0.01 [0.007–0.02]	0.01 [0.006–0.02]	0.009 [0.007–0.02]	0.739
Mean RRT, Pa^{-1}	0.30 [0.16–0.60]	0.36 [0.18–0.69]	0.25 [0.14–0.49]	0.147
Maximum transWSS, Pa	39.04 [26.50–65.55]	37.96 [25.08–67.01]	43.59 [29.83–65.88]	0.653
Minimum transWSS, Pa	0.09 [0.05–0.18]	0.09 [0.05–0.18]	0.09 [0.05–0.20]	0.443
Mean transWSS, Pa	4.58 [2.77–7.20]	3.86 [2.51–7.15]	4.96 [3.32–7.31]	0.743
Narrowed level				
Maximum TAWSS, Pa	58.67 [46.49–96.45]	55.37 [44.19–96.47]	69.69 [47.63–103.09]	0.712
Minimum TAWSS, Pa	34.09 [16.69–56.03]	32.77 [11.65–55.84]	34.18 [23.62–57.85]	0.615
Mean TAWSS, Pa	45.26 [29.49–73.92]	43.25 [24.27–74.79]	54.59 [37.01–77.15]	0.689
Maximum OSI	0.02 [0.005–0.17]	0.03 [0.01–0.20]	0.001 [0.001–0.006]	0.021*
Minimum OSI	0.002 [0.001–0.01]	0.003 [0.001–0.01]	0.001 [0.001–0.02]	0.488
Mean OSI	0.003 [0.002–0.01]	0.005 [0.001–0.02]	0.002 [0.002–0.01]	0.124
Maximum RRT, Pa^{-1}	0.03 [0.02–0.07]	0.05 [0.02–0.12]	0.03 [0.02–0.04]	0.023*
Minimum RRT, Pa^{-1}	0.02 [0.01–0.02]	0.02 [0.01–0.03]	0.01 [0.01–0.02]	0.097
Mean RRT, Pa^{-1}	0.25 [0.15–0.40]	0.32 [0.15–0.55]	0.20 [0.14–0.30]	0.266
Maximum transWSS, Pa	24.55 [19.86–39.31]	25.17 [17.45–36.64]	24.49 [21.54–40.48]	0.467
Minimum transWSS, Pa	6.23 [2.92–15.84]	4.83 [2.10–16.83]	7.20 [3.54–14.97]	0.616
Mean transWSS, Pa	14.37 [10.39–26.50]	14.22 [9.43–26.97]	15.79 [10.90–26.30]	0.545

Data are median with interquartile range (IQR). TAWSS, time-averaged wall shear stress; OSI, oscillatory shear index; RRT, relative residence time; transWSS, transverse wall shear stress. *$p < 0.05$.

Correlation of Plaque Location with Plaque Characteristics and Geometric and Hemodynamic Parameters

The results of the logistic regression analysis are detailed in Table 3. The univariate regression showed that a maximum WT, plaque length, tortuosity of the stenosed region, mean OSI, mean RRT, minimum transWSS in the proximal part, and maximum OSI and maximum RRT in the most severely NL were significantly associated with body plaques ($p < 0.05$). When the above variables were entered into a multivariate model and the model was adjusted for age and sex, tortuosity of the stenosed region (odds ratio [OR] 1.32; 95% confidence interval [CI]: 1.04, 1.66; p = 0.022), mean RRT (proximal) (OR, 0.80; 95% CI: 0.68, 0.95; p = 0.013), and minimum transWSS (proximal) (OR, 0.87; 95% CI: 0.77, 0.97; p = 0.012) remained significant factors. A comparison of these three variables is shown in Figure 4a–c. Representative cases are shown in Figure 5.

Table 3. Univariate and multivariate logistic analyses of the factors associated with body plaque of the carotid bulb

	Univariate analysis			Multivariate analysis		
	OR	95% CI	*p* value	OR	95% CI	*p* value
Maximum WT	2.42	1.44, 4.05	0.001	1.39	0.54, 3.56	0.496
Plaque length	1.14	1.02, 1.26	0.020	1.18	0.97, 1.45	0.107
Tortuosity of stenosed region	1.27	1.10, 1.46	0.001	1.32	1.04, 1.66	0.022*
Mean OSI (proximal)	0.57	0.33, 1.00	0.046	3.57	0.54, 3.95	0.111
Mean RRT (proximal)	0.98	0.95, 1.00	0.043	0.80	0.68, 0.96	0.013*
Minimum transWSS (proximal)	0.93	0.88, 0.99	0.014	0.87	0.77, 0.97	0.012*
Maximum OSI (NL)	1.30	1.00, 1.70	0.047	1.62	0.94, 2.82	0.085
Maximum RRT (NL)	1.03	1.00, 1.06	0.037	1.02	0.97, 1.07	0.455

OR, odds ratio; CI, confidence interval; WT, wall thickness; OSI, oscillatory shear index; RRT, relative residence time; transWSS, transverse wall shear stress; NL, narrowed level. *After adjustment for age, sex, and mean blood pressure.

The AUCs of tortuosity of the stenosed region, mean RRT (proximal), and minimum transWSS (proximal) for predicting the presence of body plaque were 0.78 (95% CI: 0.67, 0.87), 0.60 (95% CI: 0.48, 0.72), and 0.67 (95% CI: 0.55, 0.78), respectively. The AUC for the combination of tortuosity of the stenosed region, mean RRT (proximal), and minimum transWSS (proximal) was 0.93 (95% CI: 0.84, 0.98). The combination had a significantly higher AUC than tortuosity of the stenosed region (Z, 3.02; 95% CI: 0.05, 0.24; $p = 0.003$), mean RRT (proximal) (Z, 4.19, 95% CI: 0.17, 0.48; $p < 0.001$), and minimum transWSS (proximal) (Z, 3.63, 95% CI: 0.12, 0.39, $p < 0.001$) alone (Fig. 4d, e). Overall, the combination increased the sensitivity and specificity to approximately 90%.

Discussion

This study demonstrated plaque formation presented around the area where a decrease in the WSS value was accompanied by low flow velocity. Additionally, significant hemodynamic differences between plaque locations were found in the proximal part and the most severely NL of the plaque. Notably, the tortuosity of the stenosed region, proximal-specific RRT, and transWSS were independently associated with plaque location, and the combination of the above geometric and hemodynamic variables (compared with any variable alone) provided an incremental contribution to different plaque locations.

Previous studies have shown that low shear stress magnitude appeared to induce the development of atherosclerosis [24], but the WSS was assigned to either the upstream or downstream vessel wall in those investigations. In the present study, we analyzed the distribution of WSS magnitude at the specific most-stenosed level and further confirmed that plaque formation presented in the area where a decrease in the WSS value was accompanied by a decrease in the flow velocity. This observation is consistent with the results of a previous study reporting that WSS varies with velocity [25]. Local flow pattern around the plaque is an important mechanism for plaque formation in carotid bulb stenosis.

The tortuosity of the stenosed region was associated with the presence of body plaques in our study. A previous study suggested that geometry might influence the site of atherosclerosis development [5]. Additionally, tortuosity has been shown to be a significant and independent predictor of plaque formation in the carotid artery [19, 26]. No evidence of a difference was found in the bifurcation angle or ICA planarity between plaque locations in our study, although the above geometric variables were thought to be influential predictors of disturbed flow [9, 26]. We hypothesize that, considering the carotid geometry's potential contribution to plaque location, tortuosity might be the major parameter of interest, although the other parameters might contribute differently. Alternatively, other parameters may lack influence in patients with advanced atherosclerotic disease due to inward remodeling.

We chose to evaluate spatial differences in local hemodynamics by dividing lesions into three regions; we believe that our investigation is the first to apply

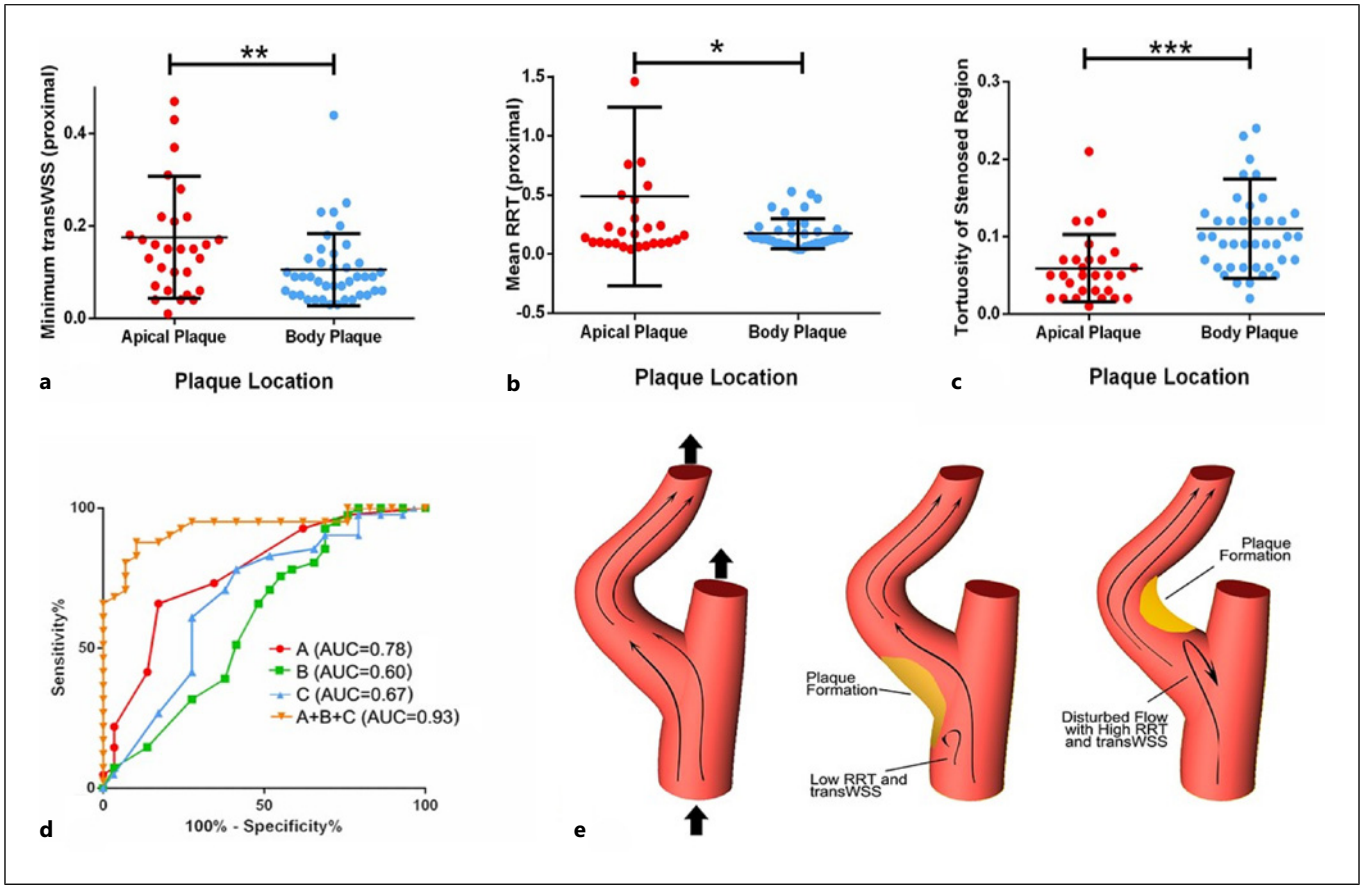

Color version available online

Fig. 4. a–c Comparison between groups with body and apical plaques in tortuosity of the stenosed region, mean RRT (proximal), and minimum transWSS (proximal) ($p < 0.05$). **d** ROC curve for determining the presence of body plaque. The combination of tortuosity of the stenosed region (**a**), mean RRT (proximal) (**b**), and minimum transWSS (proximal) (**c**) improved the AUC to 0.93 (0.84–0.98), which was significantly higher than that obtained with each variable alone (vs. tortuosity of the stenosed region, mean RRT [proximal], and minimum transWSS [proximal]: $p = 0.003$, $p < 0.001$, and $p < 0.001$, respectively). **e** Working hypothesis for the interplay between wall shear stress and plaque location. RRT, relative residence time; transWSS, transverse wall shear stress; ROC, receiver operating characteristic; AUC, area under curve. *$p < 0.05$, **$p < 0.01$, ***$p < 0.001$.

this differentiation to the carotid bulb. Our study showed that the hemodynamics in the proximal and most severely narrowed stenosis regions were the main influencing factors of plaque location. We hypothesize that different plaque locations have unique histological and anatomic features and are differentially exposed to disturbed flow [27]. Additionally, we found that RRT was related to plaque location in the carotid bulb. Previous work has shown that RRT demonstrates temporal fluctuations [28]; body plaques are mainly located in the local dilation of ICA [29], which is known to promote more flow separation. We infer that the greater increased pressure gradient induced by the body plaque pathology results in lower residence time than apical plaque. In addition, we also found that transWSS played an important role in plaque location. transWSS represents a multidirectional disturbed blood flow, which may be indicative of vascular wall dysfunction [30]. Interestingly, a previous report suggested that the highest transWSS values were observed at uncommon locations for atherosclerosis [16]. Because it is well known that body plaque occurs more frequently than apical plaque, our results further confirmed that apical plaques exhibited higher transWSS than body plaques.

There are some limitations to this study. First, like most human studies on hemodynamics and atherosclerosis, the present work was a cross-sectional study. Nevertheless, geometry, hemodynamics, and plaque are influenced by each other. Local WSS is dependent on vascular

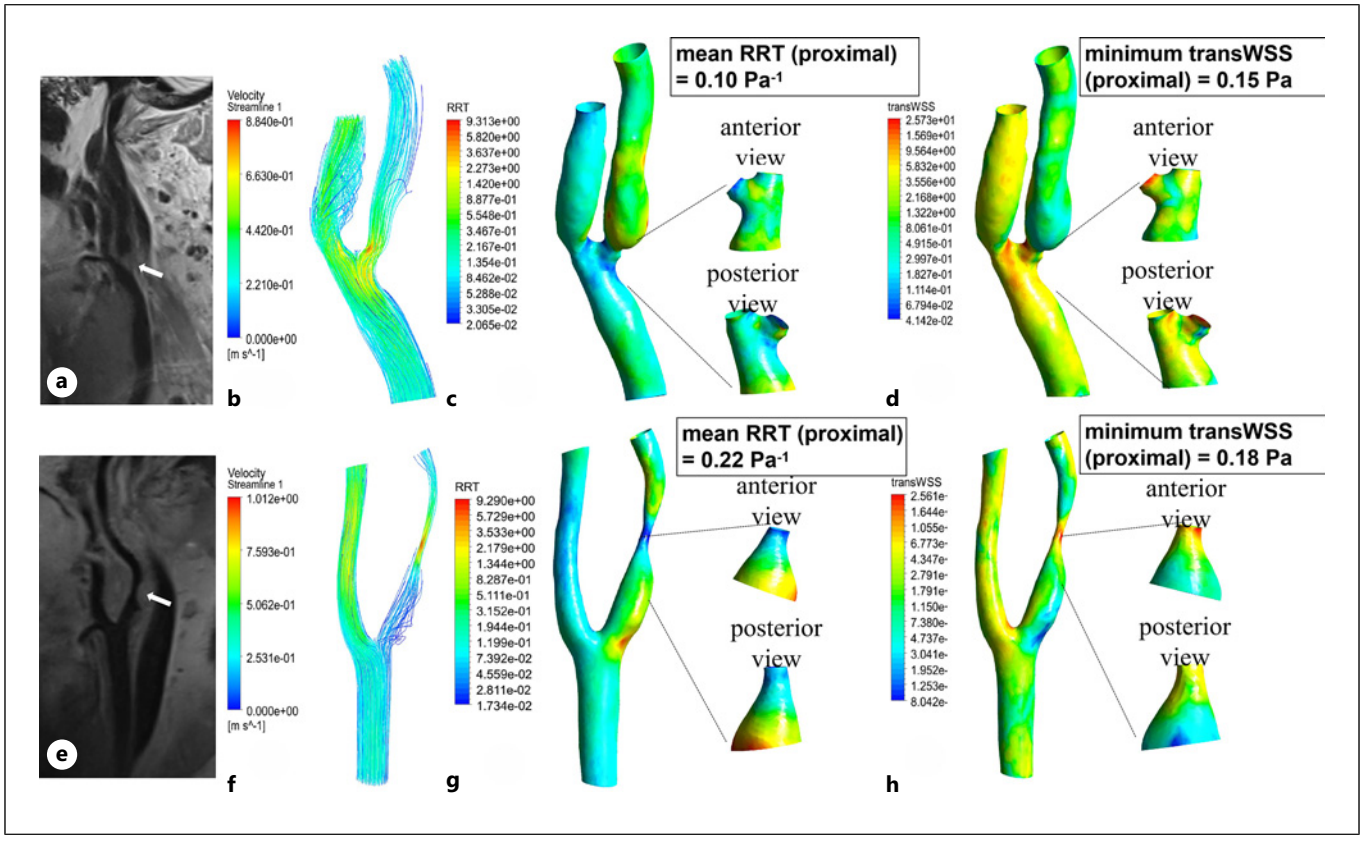

Fig. 5. Two carotid bulb stenosis cases with distinct plaque locations. Upper: body plaque. **a** HR-VWI showed the body plaque (arrow). **b** Streamlines showed no obvious disturbed flow in the proximal part of the lesion. **c** Mean RRT in the proximal part of the lesion was 0.10 Pa^{-1}. **d** Minimum transWSS in the proximal part of the lesion was 0.15 Pa. Lower: apical plaque. **e** HR-VWI showed apical plaque (arrow). **f** Streamlines showed a large disturbance in the flow in the proximal part of the lesion. **g** Mean RRT in the proximal part of the lesion was 0.22 Pa^{-1}. **h** Minimum transWSS in the proximal part of the lesion was 0.18 Pa. HR-VWI, high-resolution vessel wall imaging; RRT, relative residence time; transWSS, transverse wall shear stress.

geometry, and the vascular response to plaque formation or plaque growth induces a change in geometry, which in turn leads to changes in the local WSS [16]. Therefore, this specific relationship during plaque formation and progression deserves further investigation in a larger sample and prospective validation is needed. Second, our study only quantified WSS in patients with moderate and severe stenoses (50–99%), this study design limited the present study, the predictive value of specific hemodynamics for plaque formation and location in the carotid bulb will have to be explored by further research, normal subject should be included, and longitudinal research is warranted. Finally, non-Newtonian fluid models incorporating patient-specific boundary conditions (e.g., phase contrast flow), and blood properties are needed in future simulations to increase the accuracy of WSS quantification.

Conclusion

Our findings suggest that plaque formation is associated with the local flow pattern and that the tortuosity of the stenosed region and proximal-specific hemodynamics are significantly associated with plaque location in the carotid bulb. Our study represents a step forward in utilizing CFD based on noninvasive vascular imaging for studying the hemodynamic features of carotid bulb atherosclerotic stenosis disease. The current findings should be confirmed in large series with more patient-specific data in carotid blood flow simulations, and further in-depth studies in this area could lead to a better understanding of the pathophysiological processes and mechanisms of atherosclerotic stenosis, perhaps ultimately providing new references for the clinical risk stratification of such patients.

Acknowledgments

We thank the School of Life Science, Beijing Institute of Technology, for providing computing resources.

Statement of Ethics

This study protocol was reviewed and approved by the Ethics Committee of Tianjin First Central Hospital, approval number 2018N003KY, and conforms to the ethical guidelines of the 1975 Declaration of Helsinki. Written informed consent was obtained from each patient or their designated proxy.

Conflict of Interest Statement

The authors declare no conflict of interest.

Funding Sources

This research was funded by the Natural Scientific Foundation of China (Grant No. 82171916, 81871342), the Natural Scientific Foundation of Tianjin (Grant No. 21CYBJC01580), Tianjin Health Science and Technology Project (specific projects of key disciplines) (Grant No. TJWJ2022XK019), Tianjin Key Medical Discipline (Specialty) Construction Project (Grant No. TJYXZDXK-041A), Tianjin Municipal Human Resources and Social Security Bureau (Grant No. XB202008), and key project of the Tianjin Municipal Science and Technology Bureau, China (Grant No. 19JCZDJC35400).

Author Contributions

Conceptualization and writing – original draft preparation: Lei Ren. Methodology: Lei Ren, Rongjie Xu, and Chenxi Zhao. Software: Wenfei Li and Shu Wang. Validation: Chen Cao and Yan Gong. Formal analysis: Jinxia Zhu. Investigation: Xuequan Feng. Resources: Bo Ren. Data curation: Shuang Xia. Writing – review and editing: Shuang Xia and Bo Ren. Visualization: Rongjie Xu. Supervision: Chenxi Zhao. Project administration: Shu Wang. Funding acquisition: Shuang Xia, Shu Wang, Chen Cao, and Xuequan Feng. All authors have read and agreed to the published version of the manuscript.

Data Availability Statement

Data can be requested from the corresponding author.

References

1 GBD 2016 Neurology Collaborators. Global, regional, and national burden of neurological disorders, 1990–2016: a systematic analysis for the Global Burden of Disease Study 2016. Lancet Neurol. 2019;18(5):459–80.
2 Fereydooni A, Gorecka J, Xu J, Schindler J, Dardik A. Carotid endarterectomy and carotid artery stenting for patients with crescendo transient ischemic attacks: a systematic review. JAMA Surg. 2019;154(11):1055–63.
3 Park ST, Kim JK, Yoon KH, Park SO, Park SW, Kim JS, et al. Atherosclerotic carotid stenoses of apical versus body lesions in high-risk carotid stenting patients. AJNR Am J Neuroradiol. 2010;31(6):1106–12.
4 Lu M, Cui Y, Peng P, Qiao H, Cai J, Zhao X. Shape and location of carotid atherosclerotic plaque and intraplaque hemorrhage: a high-resolution magnetic resonance imaging study. J Atheroscler Thromb. 2019;26(8):720–7.
5 Woo HG, Heo SH, Kim EJ, Chang DI, Song TJ, Kim BJ. Atherosclerotic plaque locations may be related to different ischemic lesion patterns. BMC Neurol. 2020;20(1):288.
6 Gao S, van 't Klooster R, van Wijk DF, Nederveen AJ, Lelieveldt BPF, van der Geest RJ. Repeatability of in vivo quantification of atherosclerotic carotid artery plaque components by supervised multispectral classification. MAGMA. 2015;28(6):535–45.
7 Watase H, Sun J, Hippe DS, Balu N, Li F, Zhao X, et al. Carotid artery remodeling is segment specific: an in vivo study by vessel wall magnetic resonance imaging. Arterioscler Thromb Vasc Biol. 2018;38(4):927–34.
8 Benitez J, Fontanarosa D, Wang J, Paritala PK, McGahan T, Lloyd T, et al. Evaluating the impact of calcification on plaque vulnerability from the aspect of mechanical interaction between blood flow and artery based on MRI. Ann Biomed Eng. 2021;49(4):1169–82.
9 Phan TG, Beare RJ, Jolley D, Das G, Ren M, Wong K, et al. Carotid artery anatomy and geometry as risk factors for carotid atherosclerotic disease. Stroke. 2012;43(6):1596–601.
10 Markl M, Wegent F, Zech T, Bauer S, Strecker C, Schumacher M, et al. In vivo wall shear stress distribution in the carotid artery: effect of bifurcation geometry, internal carotid artery stenosis, and recanalization therapy. Circ Cardiovasc Imaging. 2010;3(6):647–55.
11 Lee SW, Antiga L, Spence JD, Steinman DA. Geometry of the carotid bifurcation predicts its exposure to disturbed flow. Stroke. 2008;39(8):2341–7.
12 Sitzer M, Puac D, Buehler A, Steckel DA, von Kegler S, Markus HS, et al. Internal carotid artery angle of origin: a novel risk factor for early carotid atherosclerosis. Stroke. 2003;34(4):950–5.
13 Gallo D, Bijari PB, Morbiducci U, Qiao Y, Xie YJ, Etesami M, et al. Segment-specific associations between local haemodynamic and imaging markers of early atherosclerosis at the carotid artery: an in vivo human study. J R Soc Interface. 2018;15(147):20180352.
14 Cicha I, Worner A, Urschel K, Beronov K, Goppelt-Struebe M, Verhoeven E, et al. Carotid plaque vulnerability: a positive feedback between hemodynamic and biochemical mechanisms. Stroke. 2011;42(12):3502–10.
15 Jing L-N, Gao P-Y, Lin Y, Sui B-B, Qin H-Q, Ma L, et al. Distribution of wall shear stress in carotid plaques using magnetic re sonance imaging and computational fluid dynamics analysis: a preliminary study. Chin Med J. 2011 May;124(10):1465–9.
16 Gallo D, Steinman DA, Morbiducci U. Insights into the co-localization of magnitude-based versus direction-based indicators of disturbed shear at the carotid bifurcation. J Biomech. 2016;49(12):2413–9.
17 Murata K, Murata N, Chu B, Watase H, Hippe DS, Balu N, et al. Characterization of carotid atherosclerotic plaques using 3-dimensional MERGE magnetic resonance imaging and correlation with stroke risk factors. Stroke. 2020;51(2):475–80.

18 Hatsukami TS, Ross R, Polissar NL, Yuan C. Visualization of fibrous cap thickness and rupture in human atherosclerotic carotid plaque in vivo with high-resolution magnetic resonance imaging. Circulation. 2000; 102(9):959–64.
19 Strecker C, Krafft AJ, Kaufhold L, Hullebrandt M, Weber S, Ludwig U, et al. Carotid geometry is an independent predictor of wall thickness: a 3D cardiovascular magnetic resonance study in patients with high cardiovascular risk. J Cardiovasc Magn Reson. 2020; 22(1):67.
20 Jiang P, Chen Z, Hippe DS, Watase H, Sun B, Lin R, et al. Association between carotid bifurcation geometry and atherosclerotic plaque vulnerability: a Chinese atherosclerosis risk evaluation study. Arterioscler Thromb Vasc Biol. 2020;40(5):1383–91.
21 Huang X, Yin X, Xu Y, Jia X, Li J, Niu P, et al. Morphometric and hemodynamic analysis of atherosclerotic progression in human carotid artery bifurcations. Am J Physiol Heart Circ Physiol. 2016;310(5):H639–47.
22 Wang J, Paritala PK, Mendieta JB, Gu Y, Raffel OC, McGahan T, et al. Carotid bifurcation with tandem stenosis-a patient-specific case study combined in vivo imaging, in vitro histology and in silico simulation. Front Bioeng Biotechnol. 2019;7:349.
23 Demirel S, Chen D, Mei Y, Partovi S, von Tengg-Kobligk H, Dadrich M, et al. Comparison of morphological and rheological conditions between conventional and eversion carotid endarterectomy using computational fluid dynamics: a pilot study. Vascular. 2015; 23(5):474–82.
24 Shaaban AM, Duerinckx AJ. Wall shear stress and early atherosclerosis: a review. AJR Am J Roentgenol. 2000;174(6):1657–65.
25 Li X, Sun B, Zhao H, Ge X, Liang F, Li X, et al. Retrospective study of hemodynamic changes before and after carotid stenosis formation by vessel surface repairing. Sci Rep. 2018;8(1):5493.
26 Bijari PB, Wasserman BA, Steinman DA. Carotid bifurcation geometry is an independent predictor of early wall thickening at the carotid bulb. Stroke. 2014;45(2):473–8.
27 Carvalho JL, Nielsen JF, Nayak KS. Feasibility of in vivo measurement of carotid wall shear rate using spiral Fourier velocity encoded MRI. Magn Reson Med. 2010;63(6):1537–47.
28 Malota Z, Glowacki J, Sadowski W, Kostur M. Numerical analysis of the impact of flow rate, heart rate, vessel geometry, and degree of stenosis on coronary hemodynamic indices. BMC Cardiovasc Disord. 2018;18(1):132.
29 Domanin M, Gallo D, Vergara C, Biondetti P, Forzenigo LV, Morbiducci U. Prediction of long term restenosis risk after surgery in the carotid bifurcation by hemodynamic and geometric analysis. Ann Biomed Eng. 2019; 47(4):1129–40.
30 Zhang Q, Gao B, Gu K, Chang Y, Xu J. The study on hemodynamic effect of varied support models of BJUT-II VAD on coronary artery: a primary CFD study. ASAIO J. 2014; 60(6):643–51.